Joint Communication and Sensing Design for Multihop RIS-Aided Communication Systems in Underground Coal Mines

Tianhao Guo, *Member, IEEE*, Yujie Wang, Lexi Xu, *Senior Member, IEEE*, Muyu Mei, Jia Shi, *Member, IEEE*, Lei Dong, *Member, IEEE*, Yongjun Xu, *Senior Member, IEEE*, and Chongwen Huang, *Member, IEEE*

***Abstract*—How to achieve reliable communication and safety monitoring is very important in coal mines. However, most of the existing transmission strategies and sensing-based monitoring approaches assume a single objective and neglect non-line-of-sight (NLOS) problems brought by winding tunnels or mine collapses. To this end, we first propose a multihop reconfigurable intelligent surface (RIS)-aided joint communication and sensing (JCAS) approach to maximize the energy efficiency of the JCAS access point and the sum sensing rates in order to improve the sensing accuracy. Specifically, we formulate an energy-efficient optimization problem by jointly designing both the phase-shift matrix and the switches status of the RISs as well as the transmit power of the access point. The problem is solved by adopting the successive convex approximation-based alternating optimization algorithm, the second-order optimization method, the Lambert-*w* function, and Newton's method. Moreover, a sensing-based rate optimization problem is also solved via the Lagrange relaxation method and the Gradient descent method. Simulation results demonstrate that the proposed algorithm has better robustness and higher energy efficiency.**

***Index Terms*—Disaster robustness and rescue, energy efficiency, joint communication and sensing (JCAS), reconfigurable intelligent surface (RIS), safety monitoring.**

Manuscript received 12 February 2023; revised 29 March 2023; accepted 11 April 2023. Date of publication 26 April 2023; date of current version 7 November 2023. This work was supported in part by the China National Key Research and Development Program under Grant 2021YFA1000500; in part by the National Natural Science Foundation of China under Grant 62101492; in part by the Zhejiang Provincial Natural Science Foundation of China under Grant LR22F010002; in part by the National Natural Science Fund for Excellent Young Scientists Fund Program (Overseas); in part by the Zhejiang University Global Partnership Fund; in part by the Zhejiang University Education Foundation Qizhen Scholar Foundation; in part by the Fundamental Research Funds for the Central Universities under Grant 2021FZZX001-21; in part by the National Natural Science Foundation of China under Grant 62271094; in part by the Scientific and Technological Research Program of Chongqing Municipal Education Commission under Grant KJZD-K202200601; and in part by the China Postdoctoral Science Foundation under Grant 2022MD723725. *(Corresponding author: Yongjun Xu.)*

Tianhao Guo is with the Department of Physical and Electronic Engineering, Shanxi University, Taiyuan 030006, China, and also with the National Key Laboratory of Integrated Services Networks, Xidian University, Xi'an 710071, China (e-mail: tianhao_guo@sxu.edu.cn).

Yujie Wang is with the Department of Physical and Electronic Engineering, Shanxi University, Taiyuan 030006, China (e-mail: 996725223@qq.com).

Lexi Xu is with the Research Institute, China United Network Communications Corporation, Beijing 100048, China (e-mail: davidlexi@hotmail.com).

Muyu Mei and Jia Shi are with the National Key Laboratory of Integrated Services Networks, Xidian University, Xi'an 710071, China (e-mail: mei_muyu@163.com; jiashi@xidian.edu.cn).

Lei Dong is with the Department of State Key Laboratory of Quantum Optics and Quantum Optics Devices, Institute of Laser Spectroscopy, Shanxi University, Taiyuan 030006, China (e-mail: donglei@sxu.edu.cn).

Yongjun Xu is with the School of Communication and Information Engineering, Chongqing University of Posts and Telecommunications, Chongqing 400065, China (e-mail: xuyj@cqupt.edu.cn).

Chongwen Huang is with the College of Information Science and Electronic Engineering, Zhejiang University, Hangzhou 310027, China, also with the Zhejiang-Singapore Innovation and AI Joint Research Lab, Hangzhou 310058, China, and also with the Zhejiang Provincial Key Laboratory of Info. Proc., Commun. and Netw., Hangzhou 310027, China (e-mail: chongwenhuang@zju.edu.cn).

Digital Object Identifier 10.1109/JIOT.2023.3269947

I. Introduction

COAL is the cornerstone of the energy system and the guarantee of energy security. However, the geological conditions of the coal mine environment are subject to unpredictable changes, causing three kinds of dangers during coal mining process: water seepage, goafs, and toxic and explosive gases [1], [2]. Therefore, it is necessary to design a proper communication system to guarantee safety monitoring (sensing) and communication in various severe conditions, and to forecast dangers, support rescue activities, and increase productivity.

However, the complex structure and abundant bends in the mine tunnels make the wired networks less scalable and costly to deploy and maintain. Also, the wireless networks suffer severe fading and power supply problems in nonline-of-sight (NLOS) propagation scenarios. Moreover, with the proceeding of the mining, the tunnels continue to extend forward or turn to another direction, which means that the base station (BS) needs to keep moving to provide services of communication or perception. As a result, the extending and winding tunnels bring many difficulties to the deployment of the communication and perception infrastructure. Furthermore, as the BS is moving, a dedicated line for the power supply might be "luxury" and inconvenient, and the BS might be useless for rescue activities if a disaster cut down the power line.

A. Related Works

Traditionally, the safety monitoring system in coal mines needs to deploy a large number of sensors to upload the sensory data on time [3]. Since the tunnels are advancing during the mining process, wireless sensor networks (WSNs) are better than wired sensor networks because of easy deployment and scalability. Multihop routing is necessary for WSNs since direct wireless transmission is unfeasible in the NLOS environment [4], [5]. However, the deployment and maintenance for WSNs are relatively high and not energy efficient. Moreover, WSNs cannot provide communication services for workers and facilities in the underground coal mine.

In high-frequency bands (300 MHz to 3 GHz), Wireless electromagnetic wave attenuation characteristics for underground coal mines have been investigated in various cases (rock roughness [6] and dust concentration). The feasibility of multiple-input multiple-output (MIMO) systems operating at 60 GHz (millimeter wave (mm-Wave) with higher sensing resolution) has also been proved in the real-world underground gold mines [7] in Quebec, Canada. For an MIMO system equipped with a 2×2 antenna array, the channel capacity is feasible to reach at least 4 bits/s/Hz. There is few research on terahertz (THz) propagation in mine but [8] has proved that multihop reconfigurable intelligent surfaces (RISs) can extend THz propagation. 2-D or 3-D profiling visualization systems enabled by mm-Wave or laser have been implemented in underground and surface mines in Australia and South Africa decades ago [9], [10], [11]. By monitoring the 2-D and 3-D cloud images of mining vehicles [9], [10], tunnels, dig areas, and buckets, the automation and safety can be guaranteed. By profiling visualization, scalable safety monitoring can be implemented easily. However, mechanized and automated coal mining should not only consider safety monitoring, but also need to take communication for disaster rescue and productivity into consideration.

B. Motivations and Contributions

Most of the existing works assume that the transmission via the line-of-sight (LOS) propagation is always impractical in the actual coal-mine communication scenario [12]. For example, when the transmission links are blocked by tunnels and obstacles in such scenario, the communication quality is worse. Additionally, when a disaster happens somewhere in the tunnel, the communication links, especially backhaul links to the core networks on the ground, will be blocked, which will bring troubles for rescue activities.

To solve the above challenges, we first introduce the multihop RISs [13], [14], [15], [16], [17], [18], [19] activated by switches in the coal mine communication systems in this work. As a candidate technology of 6G, the RIS technology is promising to be applied in coal mines [20]. First, since there is only one operator in the coal mine which is easy for deployment and management, RISs can be placed as the tunnels extend or turn to another direction. Second, RISs are more energy efficient and economical than WSNs [21], [22], or other relay solutions [23]. Last but not least, multihop RISs [8] are able to form multiple paths, which can be used as backup paths after a mine disaster, so that the communication system will not be paralyzed. Even if the backup paths are blocked, multihop RISs can identify the blocked link and quickly locate the collapse.

Moreover, the existing works only considered a single function, such as communication, positioning, or sensing in the coal mines. That is to say, the joint design of wireless communication and sensing in coal-mine communication systems has barely been considered. To improve communication quality as well as sensing functionality in coal-mine communication systems, we further design the joint communication and sensing (JCAS) [24], [25], [26], [27], [28], [29] problem in this article. In this way, it is expected to improve the whole system performance of coal-mine communication systems.

To improve the energy efficiency of the transmission and sensing accuracy of the multihop RISs-aided JCAS system, and to investigate the feasibility of a small battery-powered wireless backhaul BS, in this article, we study the energy-efficiency optimization problem for the communication functionality and maximize the sensing rate for the perception functionality. The main contributions are given as follows.

1) We build a multihop RISs-aided JCAS system in the underground coal mine scenario. In such scenario, we investigate the feasibility and prospect of RIS application in coal mine communication. We first apply the multihop and multipath RISs with switches in the coal mine scenario, and compare the application with the traditional amplify-and-forward (AF) relay method [23]. The result shows that RISs-aided application can realize the wireless communication relay scheme with less energy and cost. We also study a perception model in the coal mine scenario to improve the perception rate.
2) In order to maximize the energy efficiency [30] of the communication phase, we transform the problem of communication phase into joint optimization of the phase shift matrix [31], the transmit power, and RISs switches. For the phase shift matrix optimization subproblem, we use the successive convex approximation (SCA)-based alternating optimization algorithm to find the local optimal phase. For the power optimization subproblem, the local optimal transmit power is obtained by the Lambert-w function and Newton's method. For the RISs switches optimization subproblem, the optimal solution is obtained using the bitwise operation. In order to solve the problem of perceptual model, we use the Lagrange relaxation to solve nonconvex problems, and we use the gradient descent method to maximize the total perceived rate under the constraints of perceptual accuracy.
3) Simulation results show that the energy efficiency of the multihop RISs scheme with switches is 40% higher than that of the traditional AF relay, and verify the feasibility of the perceptual model in the coal mine scenario.

The remainder of this article is organized as follows. Section II introduces the system model of this article. Sections III and IV provide the problem formulation. Complexity analysis is presented in Section V. Simulation results and discussion are given in Section VI, and Section VII concludes this article.

Notations: Bold case letters denote matrices. $(\cdot)^*$, $(\cdot)^{\mathrm{T}}$, and $(\cdot)^{\mathrm{H}}$ denote the conjugate, transpose, and conjugate transpose of the matrices, respectively. $\mathrm{diag}(\cdot)$ denotes the diagonal

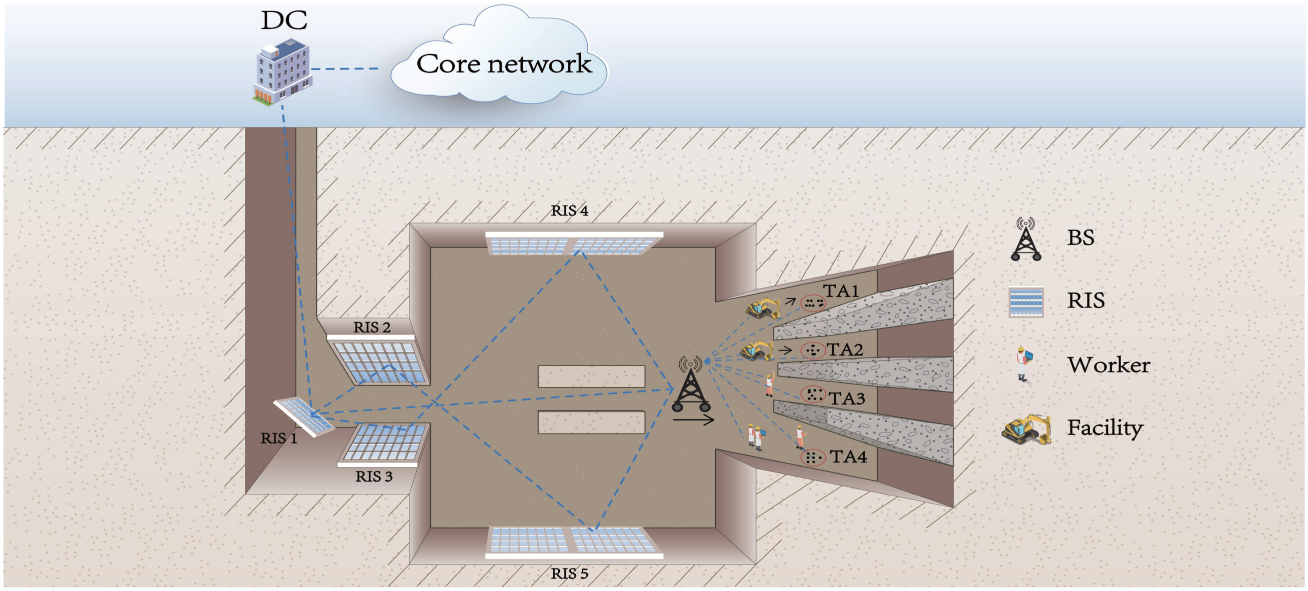

Fig. 1. Multihop RISs-aided JCAS in coal mine.

matrix. $|\cdot|$ denotes the absolute value. $\mathbb{C}^{M\times N}$ denotes matrices of $M \times N$. $\log_2(\cdot)$ and $\ln(\cdot)$ denote the logarithmic function.

II. System Model

As shown in Fig. 1, we consider an RISs-assisted coal mine JCAS system that is composed of a BS, a data center (DC) with the ability of edge computing [32], and multiple RISs. The BS senses multiple target areas (TAs) and sends the sensory data to the DC via the RISs. The DC gives the safety level and sends control signals with safety priorities to BS to adjust the frequency of sensing for TAs. In this scenario, sensory data is transmitted via RISs to avoid obstacles. Meanwhile, the BS also provides data communication services for workers and facilities in the coal mine and the DC is linked to the Internet. Considering that activating all RISs may lead to unnecessary power loss, we adopt multihop RISs with switches to transmit sensory and communication data. Table I lists the main notations for problem formulation on the next page.

We assume that the frequency of channel fading is flat. We focus on a DC-BS transmission pair wherein the DC is equipped with a single antenna and the BS is equipped with M antennas. Signals travel through L paths for the sensory data transmission. There are K_l RISs in lth path and each RIS is equipped with N reflecting elements. Furthermore, we adopt an indicator x_l to denote the switch status of the lth path with $x_l = 0$ for inactive state and $x_l = 1$ for active state. The beamforming vector [33] for DC is denoted by $\omega \in \mathbb{C}^1$, and the signals received at the BS can be written as follows:

$$y = \left(\boldsymbol{g}^{\mathrm{H}} + \sum_{l=1}^{L} x_l \boldsymbol{h}_l^{\mathrm{H}} \left(\prod_{i=1}^{K_l-1} \boldsymbol{\Theta}_{li} \boldsymbol{R}_{li}^{\mathrm{H}}\right) \boldsymbol{\Theta}_{lK_l} \boldsymbol{G}_l\right) \omega + n_c \quad (1)$$

where the vector $\boldsymbol{g} \in \mathbb{C}^{M\times 1}$ and $\boldsymbol{h}_l \in \mathbb{C}^{N\times 1}$ are the direct channel gains from the DC to BS and from the first RIS to the DC on the lth path, respectively. The vector $\boldsymbol{G}_l \in \mathbb{C}^{N\times M}$ is the channel gain from the last RIS to BS on the lth path. Also, $\boldsymbol{R}_{li} \in \mathbb{C}^{N\times N}$ is the channel gain between the ith RIS and the $(i+1)$th RIS of the lth path. $\boldsymbol{\theta}_{li} = [e^{j\theta_{li1}}, e^{j\theta_{li2}}, \ldots, e^{j\theta_{liN}}]^{\mathrm{T}}$ denotes the ith phase shift matrix on the lth path, $\boldsymbol{\Theta}_{li} = \mathrm{diag}(e^{j\theta_{li1}}, e^{j\theta_{li2}}, \ldots, e^{j\theta_{liN}})$ is the diagonal matrix of $\boldsymbol{\theta}_{li}$, and we have $|e^{j\theta_{lin}}|^2 = 1$, $n \in N$. $\boldsymbol{\theta}_{lK_l}$ denotes the phase shift matrix between the last RIS and the BS on the lth path, which is given by $\boldsymbol{\theta}_{lK_l} = [e^{j\theta_{lK_l1}}, e^{j\theta_{lK_l2}}, \ldots, e^{j\theta_{lK_lN}}]^{\mathrm{T}}$. $\boldsymbol{\Theta}_{lK_l} = \mathrm{diag}(e^{j\theta_{lK_l1}}, e^{j\theta_{lK_l2}}, \ldots, e^{j\theta_{lK_lN}})$ is the diagonal matrix of $\boldsymbol{\theta}_{lK_l}$. n_c is the Gaussian white noise with mean 0 and variance σ^2.

TABLE I
List of Notations

Notations	Meanings
M	Number of antennas in the BS
L	Number of transmission paths
K_l	Number of RISs in l^{th} path
N	Number of reflection elements on each RIS
γ	SNR of communication phase
θ	Phase shift matrix
$P_{\max}$	Maximum transmit power
$P_{\min}$	Minimum transmit power
$\bar{p}$	Optimal transmit power
n_c	Background noise
x_l	Switch status of the l^{th} path
D	Number of TAs
p_{si}	The transmit power of the sensing phase
p_{ei}	The power of echo signals
λ	Wavelength of transmit signal
d	Distance from base station to target area
G	The launch of gain
ξ	The RCS of the target
P_m	Total perceived power maximum
n_i	The i^{th} TA Background noise
δ_i	The ranging accuracy of the i^{th} TA

According to (1), the signal-to-noise ratio (SNR) at the BS can be expressed as follows:

$$\gamma = \frac{\left|\boldsymbol{g}^{\mathrm{H}} + \left(\sum_{l=1}^{L} x_l \boldsymbol{h}_l^{\mathrm{H}} \left(\prod_{i=1}^{K_l-1} \boldsymbol{\Theta}_{li} \boldsymbol{R}_{li}^{\mathrm{H}}\right) \boldsymbol{\Theta}_{lK_l} \boldsymbol{G}_l\right)\omega\right|^2}{\sigma^2}. \tag{2}$$

The total power consumption of the system P_t includes the transmit power of the DC p, which is given by $p = |\omega|^2$, the circuit power consumption of the DC P_D, the circuit power consumption of the BS P_B, the power consumption of all RISs. The power consumption of each RIS which is denoted by P_R. Thus, P_t can be calculated as follows:

$$P_t = \mu p + P_B + P_D + \sum_{l=1}^{L} x_l N K_l P_R \tag{3}$$

where $\mu = v^{-1}$ and v is the efficiency of the power amplifier, $\sum_{l=1}^{L} x_l N K_l P_R$ is the power consumption of all RISs.

Our objective in this work is to maximize the energy efficiency subject to the minimum rate requirement and the total power constraint. The corresponding objective function can be written as follows:

$$\max_{\boldsymbol{\theta},p,x} \frac{B\log_2(1+\gamma)}{\mu p + P_B + P_D + \sum_{l=1}^{L} x_l N K_l P_R} \tag{4a}$$
$$\text{s.t.} \quad B\log_2(1+\gamma) \geq R_{\min} \tag{4b}$$
$$\theta_{\text{lin}} \in [0, 2\pi], n = 1, \ldots, N \tag{4c}$$
$$P_{\min} \leq p \leq P_{\max} \tag{4d}$$
$$x_l \in \{0, 1\} \tag{4e}$$

where B is the channel bandwidth, and $P_{\max}$ and $P_{\min}$ are the maximum transmit power and minimum transmit power of the DC, respectively. $R_{\min}$ is the minimum rate required for the data transmission.

III. Energy Efficiency Optimization

Since it is difficult to obtain a local optimal solution for (4a), we apply an iterative approach to reduce the complexity of the optimization problem. First, we need to optimize the phase as well as the power p, and then take the optimal phase and power into the objective function to further obtain the optimal solution of the switch x_l.

A. Joint Phase Power Optimization

1) Optimizing $\boldsymbol{\theta}$: First, we fix the state of switch x_l, and turn problem into

$$\max_{\boldsymbol{\theta},p} \frac{B\log_2\left(1 + \frac{p\left|\boldsymbol{g}^{\mathrm{H}} + \sum_{l=1}^{L} x_l \boldsymbol{h}_l^{\mathrm{H}}\left(\prod_{i=1}^{K_l-1} \boldsymbol{\Theta}_{li}\boldsymbol{R}_{li}^{\mathrm{H}}\right)\boldsymbol{\Theta}_{lK_l}\boldsymbol{G}_l\right|^2}{\sigma^2}\right)}{\mu p + P_B + P_D + \sum_{l=1}^{L} x_l N K_l P_R}. \tag{5}$$

Since both numerator and denominator of problem (5) contain the power p, we optimize $\boldsymbol{\theta}$ under a fixed value of p. The objective function for $\boldsymbol{\theta}$ optimization can be rewritten as follows:

$$\max_{\boldsymbol{\theta}} \left|\boldsymbol{g}^{\mathrm{H}} + \sum_{l=1}^{L} x_l \boldsymbol{h}_l^{\mathrm{H}} \left(\prod_{i=1}^{K_l-1} \boldsymbol{\Theta}_{li}\boldsymbol{R}_{li}^{\mathrm{H}}\right) \boldsymbol{\Theta}_{lK_l}\boldsymbol{G}_l\right|^2 \tag{6a}$$
$$\text{s.t.} \quad \theta_{\text{lin}} \in [0, 2\pi], n = 1, \ldots, N. \tag{6b}$$

To solve a problem (6a), we optimize all RISs phase shift matrices $\boldsymbol{\theta}$ for each path. To further reduce the complexity of the algorithm, the alternating optimization algorithm and the SCA method are used to find the optimal phase shift matrix $\boldsymbol{\theta}$ for all RISs. Specifically, when we optimize phase shift matrix of the first RIS, the other phase shift matrices of RISs need to be fixed. Thus, the objective function (6a) can be rewritten as follows:

$$\max_{\boldsymbol{\theta}_{l1}} \left|\boldsymbol{g}^{\mathrm{H}} + \sum_{l=1}^{L} x_l \boldsymbol{h}_l^{\mathrm{H}} \boldsymbol{\Theta}_{l1} \boldsymbol{U}_1 \boldsymbol{G}_l\right|^2 \tag{7a}$$
$$\text{s.t.} \quad \theta_{\text{lin}} \in [0, 2\pi], n = 1, \ldots, N \tag{7b}$$

where $\boldsymbol{U}_1 = \prod_{i=1}^{K_l-1} \boldsymbol{R}_{li}^{\mathrm{H}} \boldsymbol{\Theta}_{l(i+1)}$, $\boldsymbol{h}_l^{\mathrm{H}} \in \mathbb{C}^{1\times N}$ and $\boldsymbol{\Theta}_{l1}$ is a diagonal matrix. Hence, $\boldsymbol{h}_l^{\mathrm{H}} \boldsymbol{\Theta}_{l1} = \boldsymbol{\theta}_{l1}^{\mathrm{T}} \mathrm{diag}(\boldsymbol{h}_l^{\mathrm{H}})$. In order to further simplify the operation, we define

$$\boldsymbol{h}_l^{\mathrm{H}} \boldsymbol{\Theta}_{l1} \boldsymbol{U}_1 \boldsymbol{G}_l = \boldsymbol{\theta}_{l1}^{\mathrm{T}} \boldsymbol{S}_{l1} \tag{8}$$

where $\boldsymbol{S}_{l1} = \mathrm{diag}(\boldsymbol{h}_l^{\mathrm{H}})\boldsymbol{U}_1\boldsymbol{G}_l$, $\boldsymbol{S}_{l1} \in \mathbb{C}^{N\times M}$, and $\boldsymbol{\theta}_{l1} = [e^{j\theta_{l11}}, e^{j\theta_{l12}}, \ldots, e^{j\theta_{l1N}}]^{\mathrm{T}}$.

When we optimize the kth RIS phase shift matrix in lth path, the objective function (6a) can be written as follows:

$$\max_{\boldsymbol{\theta}_{lk}} \left|\boldsymbol{g}^{\mathrm{H}} + \sum_{l=1}^{L} x_l \boldsymbol{h}_l^{\mathrm{H}} \boldsymbol{U}_2 \boldsymbol{\Theta}_{lk} \boldsymbol{U}_3 \boldsymbol{G}_l\right|^2 \tag{9a}$$
$$\text{s.t.} \quad \theta_{\text{lin}} \in [0, 2\pi], n = 1, \ldots, N \tag{9b}$$

where $\boldsymbol{U}_2 = \prod_{i=1}^{k-1} \boldsymbol{\Theta}_{li}\boldsymbol{R}_{li}^{\mathrm{H}}$, $\boldsymbol{U}_3 = \prod_{i=k}^{K_l-1} \boldsymbol{R}_{li}^{\mathrm{H}}\boldsymbol{\Theta}_{l(i+1)}$, $\boldsymbol{\Theta}_{lk}$ is a diagonal matrix and $\boldsymbol{h}_l^{\mathrm{H}}\boldsymbol{U}_2 \in \mathbb{C}^{1\times N}$. Thus, we can obtain

$$\boldsymbol{h}_l^{\mathrm{H}} \boldsymbol{U}_2 \boldsymbol{\Theta}_{lk} = \boldsymbol{\theta}_{lk}^{\mathrm{T}} \mathrm{diag}\left(\boldsymbol{h}_l^{\mathrm{H}} \boldsymbol{U}_2\right). \tag{10}$$

When optimizing the phase shift matrix of the kth RIS, all $\boldsymbol{\theta}$ are fixed except the $\boldsymbol{\theta}_{lk}$. So, we define

$$\boldsymbol{h}_l^{\mathrm{H}} \boldsymbol{U}_2 \boldsymbol{\Theta}_{lk} \boldsymbol{U}_3 \boldsymbol{G}_l = \boldsymbol{\theta}_{lk}^{\mathrm{T}} \boldsymbol{S}_{lk} \tag{11}$$

where $\boldsymbol{S}_{lk} = \mathrm{diag}(\boldsymbol{h}_l^{\mathrm{H}}\boldsymbol{U}_2)\boldsymbol{U}_3\boldsymbol{G}_l$, $\boldsymbol{S}_{lk} \in \mathbb{C}^{N\times M}$ and $\boldsymbol{\theta}_{lk} = [e^{j\theta_{lk1}}, e^{j\theta_{lk2}}, \ldots, e^{j\theta_{lkN}}]^{\mathrm{T}}$.

When we try to derive the ith phase shift matrix of the RIS for path l from problem (7a), formula (8), problem (9), and formula (11), the objective function can be expressed as follows:

$$\max_{\boldsymbol{\theta}_{li}} \left|\boldsymbol{g}^{\mathrm{H}} + \sum_{l=1}^{L} x_l \boldsymbol{\theta}_{li}^{\mathrm{T}} \boldsymbol{S}_{li}\right|^2 \tag{12a}$$
$$\text{s.t.} \quad \theta_{\text{lin}} \in [0, 2\pi], n = 1, \ldots, N \tag{12b}$$

where $\boldsymbol{\theta}_{li}$ denotes the phase shift matrix of the ith RIS of the path l. Since each switch controls one transmission path, we define $\boldsymbol{S}_i = x_1\boldsymbol{S}_{1i} + \cdots + x_L\boldsymbol{S}_{Li} \in \mathbb{C}^{N\times M}$, $\boldsymbol{\phi}_{li} = \boldsymbol{\theta}_{li}^*$, and (12a) can be expressed as follows:

$$\max_{\boldsymbol{\phi}} \left|\boldsymbol{g} + \boldsymbol{S}_i^{\mathrm{H}} \boldsymbol{\phi}_{li}\right|^2 \tag{13a}$$
$$\text{s.t.} \quad |\phi_{\text{lin}}| = 1, n = 1, \ldots, N. \tag{13b}$$

To deal with the nonconvex problem (13a), the SCA method is used to approximate problem (13b) as follows:

Algorithm 1 SCA-Based Alternating Optimization Algorithm for Phase Shift Matrices

Initialize $\left(\boldsymbol{\phi}_{l1}^{(0)}, \boldsymbol{\phi}_{l2}^{(0)}, \ldots, \boldsymbol{\phi}_{lK_l}^{(0)}\right)$, iteration number $Q = 1$
repeat
  for $i = 1, \ldots, K_l$
    repeat
      Set $\boldsymbol{\phi}_{li}^{(n)} = e^{\angle \boldsymbol{S}_i\left(\boldsymbol{g}+\boldsymbol{S}_i^{\mathrm{H}}\boldsymbol{\phi}_{li}^{(n-1)}\right)}$, and $Q = Q + 1$
    until the objective value (13a) converges, and the optimal value is v_{li}.
    Set $\boldsymbol{\theta}_{li} = \left(\boldsymbol{\phi}_{li}^{(n)}\right)^*$, $\boldsymbol{\phi}_{li}^{(0)} = \boldsymbol{\theta}_{li}$
  endfor
until all the values of v_{li} are equal and converge after q iterations.
Output $\boldsymbol{\theta}_{li} = \left(\boldsymbol{\phi}_{li}^{(n)}\right)^*$.

$$\max_{\boldsymbol{\phi}} \; 2R\left(\left(\boldsymbol{g} + \boldsymbol{S}_i^{\mathrm{H}}\boldsymbol{\phi}_{li}^{(n-1)}\right)\boldsymbol{S}_i^{\mathrm{H}}\boldsymbol{\phi}_{li}\right) + \left|\boldsymbol{g} + \boldsymbol{S}_i^{\mathrm{H}}\boldsymbol{\phi}_{li}^{(n-1)}\right|^2 - 2R\left(\left(\boldsymbol{g} + \boldsymbol{S}_i^{\mathrm{H}}\boldsymbol{\phi}_{li}^{(n-1)}\right)\boldsymbol{S}_i^{\mathrm{H}}\boldsymbol{\phi}_{li}^{(n-1)}\right) \tag{14a}$$

$$\text{s.t.} \;\; |\phi_{\text{lin}}| = 1, n = 1, \ldots, N \tag{14b}$$

which is the first-order Taylor series of $|\boldsymbol{g} + \boldsymbol{S}_i^{\mathrm{H}}\boldsymbol{\phi}_{li}|^2$. The superscript $(n-1)$ indicates the value of the variable $\boldsymbol{\phi}_{li}$ at the $(n-1)$th iteration. According to (14a), to maximize the objective function, we first need to maximize $R((\boldsymbol{g} + \boldsymbol{S}_i^{\mathrm{H}}\boldsymbol{\phi}_{li}^{(n-1)})\boldsymbol{S}_i^{\mathrm{H}}\boldsymbol{\phi}_{li})$, under the circumstance that $|\phi_{\text{lin}}| = 1$. Thus, the optimal solution of problem (14a) can be obtained as follows:

$$\boldsymbol{\phi}_{li} = e^{j\angle \boldsymbol{S}_i\left(\boldsymbol{g}+\boldsymbol{S}_i^{\mathrm{H}}\boldsymbol{\phi}_{li}^{(n-1)}\right)} \tag{15}$$

where $\angle(\cdot)$ denotes the angle of a vector, which is denoted by $[\angle(\cdot)]_q = \arctan[I([\,\cdot\,]_q)/R([\,\cdot\,]_q)]$.

We bring the phase shift matrix of all RISs as initial value into the objective function (6a) and repeat the above optimization method for $\boldsymbol{\theta}$. After several iterations, we can obtain the optimal solution of $\boldsymbol{\theta}$. The SCA-based alternating optimization algorithm for solving the RISs phase shift matrices is shown in Algorithm 1.

2) Power Optimization: Take the optimal $\boldsymbol{\theta}$ solved above in problem (5) and let

$$c = \frac{\left|\boldsymbol{g}^{\mathrm{H}} + \sum_{i=1}^{L} x_l \boldsymbol{h}_l^{\mathrm{H}}\left(\prod_{i=1}^{K_l-1} \boldsymbol{\Theta}_{li}\boldsymbol{R}_{li}^{\mathrm{H}}\right)\boldsymbol{\Theta}_{lK_l}\boldsymbol{G}_l\right|^2}{\sigma^2}. \tag{16}$$

According to formula (16), problem (5) can be simplified as follows:

$$\max_{p} \; \frac{B\log_2(1+cp)}{\mu p + P_0} \tag{17a}$$

$$\text{s.t.} \;\; P_{\min} \le p \le P_{\max} \tag{17b}$$

where $P_0 = P_B + P_D + \sum_{l=1}^{L} x_l N K_l P_R$. According to Shannon's theorem which is cater for the system power requirement, the minimun transmit power can be calculated as $P_{\min} = ([2^{[(R_{\min}/B)-1]}]/c)$.

We take the derivative of problem (17a), of which derivative can be expressed as follows:

$$\frac{\partial \frac{B\log_2(1+cp)}{\mu p + P_0}}{\partial p} = \frac{B\left[c(\mu p + P_0) - \mu(1+cp)\ln(1+cp)\right]}{(1+cp)(\mu p + P_0)^2 \ln 2}. \tag{18}$$

According to (18), we can obtain

$$\begin{cases} f(p) = (1+cp)(\mu p + P_0)^2 \ln 2 & \forall p > 0 \\ g(p) = c(\mu p + P_0) - \mu(1+cp)\ln(1+cp) & \forall p > 0 \end{cases}. \tag{19}$$

For $f(p)$ in (19), we can easily find that when $p > 0$, $f(p)$ is a monotonically increasing function, and $f(p)$ is positive.

Take the first order derivative of $g(p)$ for (19) and we have

$$g'(p) = -\mu c \ln(1+cp) < 0. \tag{20}$$

The above derivative shows that $g(p)$ is a monotonically decreasing function. Since $g(0) = cP_0 > 0$ and $\lim_{p\to\infty} g(p) < 0$, there exists a $\bar{p}$ such that $g(\bar{p}) = 0$. According to (18), we need to calculate this constant, and we have

$$\frac{cP_0 - \mu}{\mu e} = \frac{1 + c\bar{p}}{e} \ln\left(\frac{1 + c\bar{p}}{e}\right). \tag{21}$$

According to the above equation, the optimal power can be calculated as follows:

$$\bar{p} = \frac{e^{w\left(\frac{cP_0 - \mu}{\mu e}\right)+1} - 1}{c} \tag{22}$$

where $w(\cdot)$ is the Lambert-w function. In summary, the objective function (17a) increases in interval $(0,\ \bar{p}]$ and decreases in interval $(\bar{p},\ +\infty)$. Thus, the objective function (17a) is maximized when $\bar{p} = ([e^{w([cP_0 - \mu/\mu e])+1} - 1]/c)$.

According to the objective function (17a) as well as the constraint (17b), the optimal power can be discussed in three cases.

1) If $\bar{p}$ lies in interval $[P_{\min},\ P_{\max}]$, the optimal transmit power can be expressed by
$$p = \left[\frac{e^{w\left(\frac{cP_0 - \mu}{\mu e}\right)+1} - 1}{c}\right]_{P_{\min}}^{P_{\max}}. \tag{23}$$
2) If $\bar{p}$ lies in interval $(0,\ P_{\min})$, then the optimal transmit power should be $P_{\min}$.
3) If $\bar{p}$ lies in interval $(P_{\max},\ +\infty)$, then the optimal transmit power should be $P_{\max}$.

Based on the above derivation, if $p \in (0, +\infty)$, the objective function (17a) is similar to a quadratic function that increases first and then decreases. Thus, there should be a maximum value of problem (17a). Here, we use Newton's method to find the optimal value of p. First, the objective function (17a) is rewritten as follows:

$$\min_{p} \; -\frac{B\log_2(1+cp)}{\mu p + P_0} \tag{24a}$$

$$\text{s.t.} \;\; P_{\min} \le p \le P_{\max}. \tag{24b}$$

To solve the above problem, we first let $p \in (0, +\infty)$, and we have

$$F(p) = -\frac{B\log_2(1+cp)}{\mu p + P_0} \quad \forall p > 0. \tag{25}$$

According to (19) and (20), the first and second order derivatives of (24a) are

$$F'(p) = \frac{\partial\left(-\frac{B\log_2(1+cp)}{\mu p + P_0}\right)}{\partial p} = -\frac{Bg(p)}{f(p)} \tag{26}$$

Algorithm 2 Newton's Method

Initialize P_0, ϵ, $P_{\min}$, $P_{\max}$, Set iteration number $I = 1$.
Calculate $F'(p)$, $F''(p)$.
repeat
  Set $p^{(I)} = p^{(I-1)} - \frac{F'(p^{(I-1)})}{F''(p^{(I-1)})}$, $I = I + 1$.
until the objective value (24a) converges.
  if $\bar{p} \leq P_{\min}$, then
    $\bar{p} = P_{min}$.
  end
  if $\bar{p} \geq P_{max}$, then
    $\bar{p} = P_{\max}$.
  end
Output $\bar{p}$.

$$F''(p) = -\frac{B}{\ln 2}\frac{q_1 - q_2}{(1+cp)^2(\mu p + P_0)^4} \tag{27}$$

where

$$q_1 = g'(p)(1+cp)(\mu p + P_0)^2 \tag{28}$$
$$q_2 = g(p)\Big[c(\mu p + P_0)^2 + 2\mu(1+cp)(\mu p + P_0)\Big]. \tag{29}$$

According to (26) and (27), we obtain the update formula of Newton's method as follows:

$$p^{(I)} = p^{(I-1)} - \frac{F'\big(p^{(I-1)}\big)}{F''\big(p^{(I-1)}\big)} \tag{30}$$

where I denotes the number of iterations, with the iteration accuracy ϵ, we stop the interation until $f'(p) \leq \epsilon$, so the optimal solution for the transmit power $\bar{p}$ can be obtained. Considering the constraint (24a), we also need to take the case that $\bar{p}$ is not in the interval $[P_{\min}, P_{\max}]$ into consideration.

If $\bar{p}$ lies in interval $(0, P_{\min})$, then the optimal transmit power should be $P_{\min}$. If $\bar{p}$ lies in interval $(P_{\max}, +\infty)$, then the optimal transmit power should be $P_{\max}$. Newton's method for solving the transmit power optimization problem is shown in Algorithm 2.

B. RISs Switches Optimization

For the optimization of the RISs switches, the optimized $\boldsymbol{\theta}$ and p are first brought into the objective function (4a) and the objective function is expressed as follows:

$$\max_{x} \quad \frac{\log_2(1+\gamma)}{\mu p + P_B + P_D + \sum_{l=1}^{L} x_l N K_l P_R} \tag{31a}$$
$$\text{s.t.} \quad B\log_2(1+\gamma) \geq R_{\min} \tag{31b}$$
$$x_l \in \{0, 1\}. \tag{31c}$$

Since the objective function in problem (31a) is discrete and nonconvex, the value of x_l is 0 or 1, it can be viewed as a 0–1 programming. Thus, we utilize the bitwise operation algorithm to solve this equivalent problem. First, we set the initial switch sequence to a zero vector, i.e., $A_0 = \{0, 0, \ldots, 0\}$, and bring the switch sequence A_0 into the objective function (31a) to obtain the function value y_0. We denote the switch sequence after xth iteration by A_x and denote $a_{x(l)} \in \{0, 1\}$ the state of the lth switch after xth iteration. Then, the sequence of switch after the $(x+1)$th iteration can be written as follows:

$$A_{x+1} = \big\{a_{x(L)}, a_{x(L-1)}, \ldots, a_{x(l)}, \ldots, a_{x(2)}, a_{x(1)} \oplus 1\big\} \tag{32}$$

Algorithm 3 Bitwise Algorithm

Set $A_0 = \{a_{x(L)}, \ldots, a_{x(l)}, \ldots, a_{x(2)}, a_{x(1)}\}$.
Initialize $a_{x(L)} = a_{x(L-1)} = \cdots = a_{x(l)} = \cdots = a_{x(2)} = a_{x(1)} = 0$.
Calculate y_0 according to A_0 and objective value (31a).
Set $A_{op} = A_0$, $y_{op} = y_0$.
for $x = 0 : (2^L - 2)$
  Set $A_{x+1} = \{a_{x+1}, \ldots, a_{x(l)}, \ldots, a_{x(2)}, \ldots, a_{x(2)}, a_{(x(1)} \oplus 1\}$.
  Calculate y_{x+1} according to A_{x+1} and objective value (31).
  if $y_{x+1} \geq y_{op}$, then
    $A_{op} = A_{x+1}$, $y_{op} = y_{x+1}$.
  end
end
Output A_{op}, y_{op}.

where A_{x+1} is the binary sequence and $\oplus$ denotes binary addition operation. Bringing the switch sequence A_x into the objective function (31a), we can obtain the value of the function which is denoted by y_x. By comparing the values of all y_x, the optimal value of the objective function can be well obtained, which is denoted by y_{op}. Meanwhile, the corresponding switch sequence of the optimal value is the optimal sequence, which is denoted by A_{op}. The bitwise algorithm to the RISs switch sequence optimization problem is shown in Algorithm 3.

IV. Sensing Rate Optimization

According to the signal perception principle [34], the relationship between the power of sensing signals (p_{si}) from BS and the power of echo signals (p_{ei}) from the ith TA can be expressed as follows:

$$p_{ei} = \frac{p_{si} G_i^2 \xi_i \lambda_i^2}{(4\pi)^3 d_i^4}. \tag{33}$$

We assume that the distance d_i from the BS to the ith TA, the transmit signal wavelength (λ_i), antenna gain (G_i), and the RCS of the target (ξ_i) are all fixed, so we can simplify (33) as (34) to express the SNR of received echo signals from ith TA

$$\text{SNR}_i = \frac{p_{ei}}{n_i} \tag{34}$$

where n_i is the Gaussian white noise with mean of 0 and variance σ_1^2.

To meet the accuracy requirements, the resolution of the ith sensed TA is

$$\delta_i = \frac{c}{2B_i\sqrt{2\,\text{SNR}_i}}. \tag{35}$$

Our objective is to maximize the total sensing rate [35] while satisfying the constraints on both accuracy and total transmit power P_m. The sensing objective function is set by

$$\max_{p_{si}} \sum_{i=1}^{D} B_i \log_2(1 + \text{SNR}_i) \tag{36a}$$
$$\text{s.t.} \sum_{i=1}^{D} \delta_i \leq \sum_{i=1}^{D} \delta_{i,\max} \tag{36b}$$

$$\sum_{i=1}^{D} p_{si} \leq \mathrm{P}_m \tag{36c}$$

where p_i is the transmit power of the signal from the BS to the ith TA. Constraint (36b) denotes the accuracy and (36c) denotes the transmit power constraint. This problem is a nonconvex optimization problem, and it can be rewritten as follows:

$$\min_{p_{si}} \ -\sum_{i=1}^{D} B_i \log_2(1+\mathrm{SNR}_i) \tag{37a}$$

$$\text{s.t.} \ \sum_{i=1}^{D} \delta_i - \sum_{i=1}^{D} \delta_{i,\max} \leq 0 \tag{37b}$$

$$\sum_{i=1}^{D} p_{si} - \mathrm{P}_m \leq 0. \tag{37c}$$

Problem (37a) can be transformed by the Lagrangian relaxation method as follows:

$$\max_{u_i \geq 0} \min_{p_{si}} \ L(p_{si}, u_i) = -\sum_{i=1}^{D} B_i \log_2(1+\mathrm{SNR}_i) + \sum_{i=1}^{D} u_i\left(\delta_i - \delta_{i,\max}\right) \tag{38a}$$

$$\text{s.t.} \ \sum_{i=1}^{D} p_{si} - P_m \leq 0 \tag{38b}$$

where u_i represents the Lagrange multiplier and we use the gradient descent method to find the optimal solution. First, we set the initial vector value by $\boldsymbol{p}_0 = [p_{1,0}, p_{2,0}, \ldots, p_{D,0}]^{\mathrm{T}}$ for the transmit power of D TA. After $(m+1)$th iterations, the optimized transmit power matrix can be written by

$$\boldsymbol{p}^{(m+1)} = \boldsymbol{p}^{(m)} + \alpha \nabla \boldsymbol{L}_{\boldsymbol{p}^{(m)}} \tag{39}$$

where $\nabla \boldsymbol{L}_{\boldsymbol{p}^{(m)}} = [(\partial L_{\boldsymbol{p}^{(m)}}/\partial p_{s1}^{(m)}), (\partial L_{\boldsymbol{p}^{(m)}}/\partial p_{s2}^{(m)}), \ldots, (\partial L_{\boldsymbol{p}^{(m)}}/\partial p_{sD}^{(m)})]^{\mathrm{T}}$, and α denotes the step size. The iteration is stopped when $p_{si}^{(m+1)} - p_{si}^{(m)} \leq \varepsilon (i = 1, 2, \ldots, D)$, where ε denotes the iteration accuracy. While optimizing the transmit power matrix $\boldsymbol{p}, u_i$ is updated simultaneously with the iterations of $\boldsymbol{p}$. Set the initial values of $u_i (i = 1, 2, \ldots, D)$ as $\boldsymbol{u} = [u_1, u_2, \ldots, u_D]$, then we have

$$\boldsymbol{u}^{(m+1)} = \max\left\{\boldsymbol{u}^{(m)} + \beta \nabla L_{u^{(m)}}, 0\right\} \tag{40}$$

where $\nabla L_{\boldsymbol{u}^{(m)}} = [(\partial L_{\boldsymbol{u}^{(m)}}/\partial u_1^{(m)}), (\partial L_{\boldsymbol{u}^{(m)}}/\partial u_2^{(m)}), \ldots, (\partial L_{\boldsymbol{u}^{(m)}}/\partial u_D^{(m)})]^{\mathrm{T}}$, and β denotes the iteration step size. The Lagrangian relaxation algorithm for solving the perceived power allocation problem is shown in Algorithm 4.

Algorithm 4 Lagrangian Relaxation Algorithm

Initialize $\boldsymbol{p}_0 = [p_{1,0}, \ldots, p_{D,0}]$, $\boldsymbol{u} = [u_1, \ldots, u_D]$, and P_m.
Set $L = -\sum_{i=1}^{D} B_i \log_2(1+SNR_i) + \sum_{i=1}^{D} u_i(\delta_i - \delta_{i,max})$, $\alpha = 0.01$, and $\beta = 0.01$.
for $T = 1 : K_D$
  Set $\boldsymbol{p}^m = \boldsymbol{p}^{(m-1)} + \alpha \bigtriangledown L_{\boldsymbol{p}^{(m-1)}}$, $\boldsymbol{u}^{(m)} = \boldsymbol{u}^{(m-1)} + \beta \bigtriangledown L_{\boldsymbol{u}^{(m-1)}}$,
  $L^{(m)} = -\sum_{i=1}^{D} B_i \log_2\left(1+\mathrm{SNR}_i^{(m-1)}\right) + \sum_{i=1}^{D} u_i^{(m-1)}\left(\delta_i - \delta_{i,\max}\right)$.
  if $p_{si}^{(m)} - \mathrm{P}_m \leq 0$, then
    continue.
  end
  if $L^{(m)} \geq L^{(m-1)}$, then
    $L = L^{(m)}$, $\boldsymbol{p} = \boldsymbol{p}^{(m)}$.
  end
end
Output $\boldsymbol{p}$, L.

V. Complexity Analysis

According to Algorithm 1, the optimization problem of solving the phase shift matrix utilizes the SCA-based alternating optimization algorithm. In this algorithm, the phase shift matrix of each RIS is optimized using the SCA method. The SCA method for solving problem (13a) requires iterations Q and $\boldsymbol{S}_i^{\mathrm{H}} \in \mathbb{C}^{M\times N}, \boldsymbol{\phi}_{li} \in \mathbb{C}^{N\times 1}$. So, performing one iteration requires computing $O(MN)$. The complexity of the SCA method is $O(\mathrm{MNQ})$, and the alternating optimization process requires $(K_l q)$ iterations. Therefore, the total arithmetic complexity of Algorithm 1 is $O(K_l qMNQ)$. According to Algorithm 2, each iteration needs to compute $F'(p)$ and $F''(p)$. When the accuracy requirement is met, the iteration stops. Thus, the total complexity of Newton's method is $O(\log_2 n)$. According to Algorithm 3, the bitwise algorithm needs to perform 2^L calculations. So, the total complexity of solving the switch sequence optimization problem (31a) is $O(2^L)$. According to Algorithms 1 and 2. we optimize the transmit power after optimizing the phase shift matrix. We consider the particularity of the coal mine scene, and the number of communication paths, the number of RISs, the number of BS antennas are all finite. Therefore, the overall complexity of the SCA-based alternating optimization algorithm and Newton's method is $O(Qq + \log_2 n)$. In the bitwise operation, each iteration needs to optimize the phase shift matrix and transmit power, so the overall complexity of the communication phase is $O[2^L(Qq + \log_2 n)]$. According to Algorithm 4, with $\boldsymbol{p} \in \mathbb{C}^{D\times 1}$ and $\boldsymbol{u} \in \mathbb{C}^{D\times 1}$, each iteration needs to be computed $2D$ times. In all, the total complexity of Algorithm 4 is $O(DK_D)$.

VI. Simulation Results and Discussion

A. Simulation Parameter Settings

In a square simulation scenario of 400×400 m^2, we utilize multihop RISs-aided JCAS system shown in Fig. 1. There are one BS, five RISs, and one DC. The number of the BS's antennas and the number of RIS's reflecting elements are both set as 4, and the DC is equipped with a single antenna. There are four communication paths between the BS and DC. Two of these paths have three RISs installed and one path has one RIS installed, which has a direct path. The maximum signal transmit power of the DC is $P_{\max} = 40$ dBm. We compare the multihop RISs scheme (labeled as "xmRIS") with the following schemes: the single-path multihop RISs scheme (labeled as "smRIS"), a conventional single-path single RIS scheme [36] (labeled as "ssRIS"), the conventional AF scheme (labeled

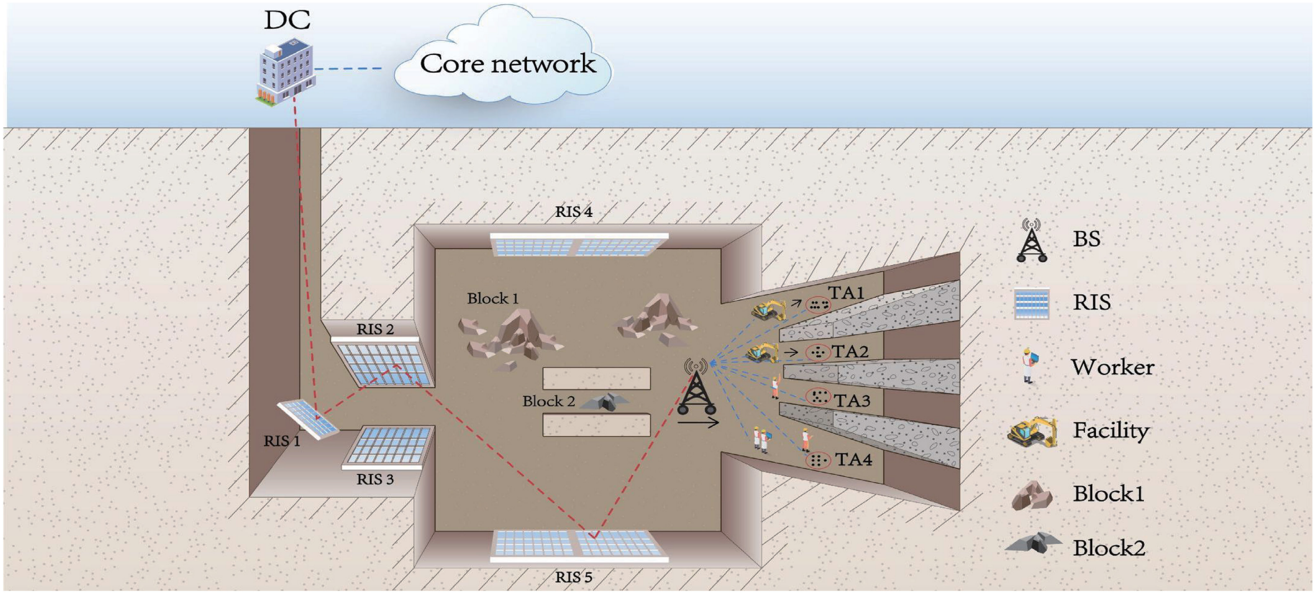

Fig. 2. Communication link blocking.

as “AF”), and the communication link blocking disaster due to collapse, wherein the collapse location is shown in Fig. 2. In the simulation, we denote the communication link blockage caused by collapse 1 and collapse 2 by “xmRISB1” and “xmRISB2,” respectively. In order to own the same deployment for all four scenarios, we set the same locations of BSs and DCs for all six scenarios. In the AF relay scenario, the AF relay is placed at the same location as the RIS adjacent to the DC, and the AF is equipped with four antennas. We set the circuit power consumption of AF relay transceiver antenna P_A to be the same as the power consumption of each reflective element on the RIS P_R. For the sensing phase, we do not consider the channel-to-channel interference. We set a total of four TAs, and the BS assigns 1 antenna to each sensing area for sensing, respectively. Each BS can serve four TAs at the same time. The main system parameters of the communication phase and the sensing phase are listed in Table II.

TABLE II
COMMUNICATION SIMULATION PARAMETER SETTING

Parameter Name	**Value**
Frequency band width B	1MHz
Noise power σ^2	−150dBm
Power Amplifier Efficiency ν	0.8
Circuit power consumption of BS P_B	20dBm
Circuit power consumption in data centres P_D	20dBm
Power consumption of each reflective element on the RIS P_R	10dBm
Circuit power consumption per AF relay transceiver antenna P_A	10dBm
Maximum transmit power of the AF relay $P_{T\ \max}$	30dBm
Frequency band width B_i	1MHz
Noise power σ_1^2	−100dBm
Total perceived power maximum P_m	100dBm
Perceptual accuracy $\delta_{i,\max}$	2m
The launch of gain G_i	45dB
The RCS of the target ξ_i	1
Wavelength of transmit signal λ_i	0.1m

B. Analysis of Simulation Results

Figs. 3 and 4 represent the convergence of two single-path multihop RISs communication links after optimizing all RISs phase shift matrices using the SCA-based alternating optimization algorithm. The normalized channel gains of the corresponding channels in Figs. 3 and 4 are “DC-RIS1-RIS2-RIS5-BS” (labeled as “channel 1”) and “DC-RIS1-RIS3-RIS4-BS” (labeled as “channel 2”), respectively. In this case, the initial values of the RISs phase shift matrices are randomized and each RIS phase shift matrix is optimized using the SCA and alternating optimization methods. The vertical coordinate represents the ratio of channel gain to noise. In these plots, we can see that the ratio increases and gradually reaches convergence as the number of iterations increases. And the three RISs optimization results in each path eventually converge to the same value, which is the closed-form solution obtained by the SCA-based alternating optimization algorithm. Considering the variation of communication environment and communication distance, the channel gains of the two paths will also vary, and the results of the two paths optimization will be different. Therefore, in practical situations, the appropriate channel should be selected for communication based on real-time channel environment and communication distance.

Fig. 5 shows the convergence comparison of Newton’s method and dichotomy. As shown in Fig. 5, the convergence values of the two algorithms are the same, indicating that the two algorithms can both maximize energy efficiency. The complexity of Newton’s method used in this article is $O(\log_2 n)$. In dichotomy, the size of each search interval is changed to 1/2

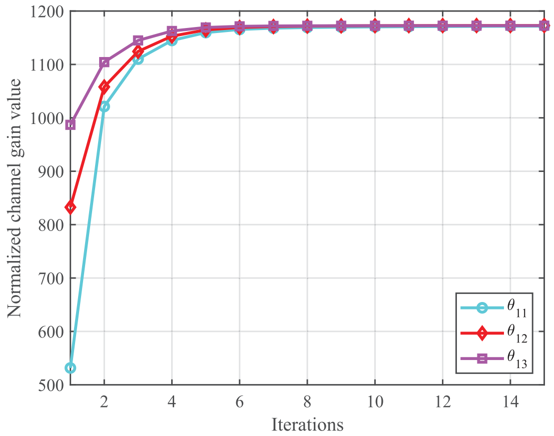

Fig. 3. Convergence under random initial values under channel 1.

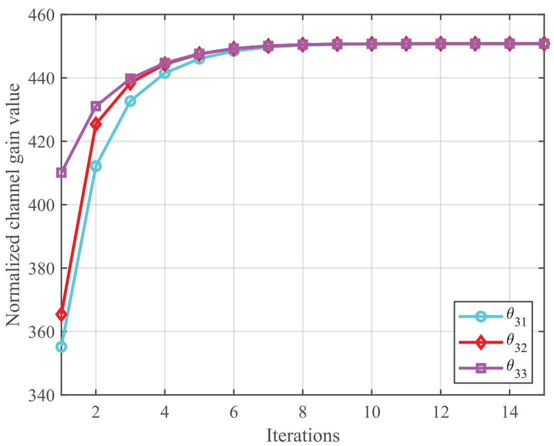

Fig. 4. Convergence under random initial values under channel 2.

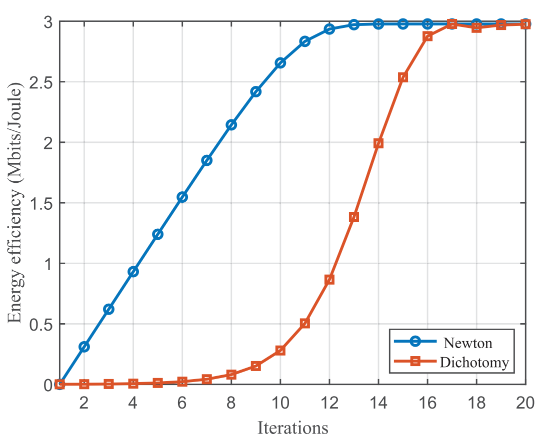

Fig. 5. Convergence comparison of two methods.

of the original. Hence, the number of dichotomies is the number of times the basic statement is executed. This information shows that the complexity of the dichotomy is $O(\log_2 n)$. Although the two algorithms have the same complexity, it can be seen from Fig. 5 that when we set the same precision for the two algorithms, the number of iterations Newton's method uses to achieve the maximum energy efficiency is fewer, indicating that the convergence rate of Newton's method used in this article is faster than the dichotomy.

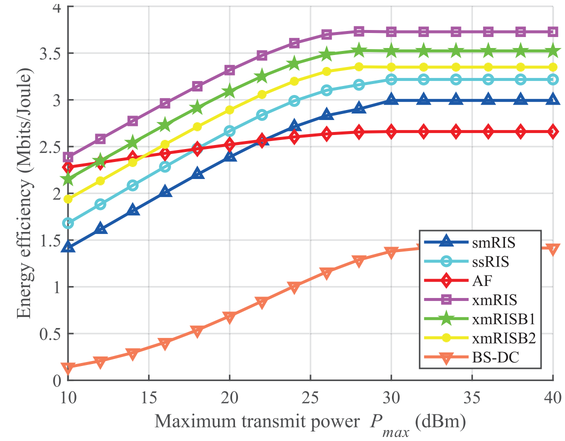

Fig. 6. Energy efficiency versus the maximum transmit power.

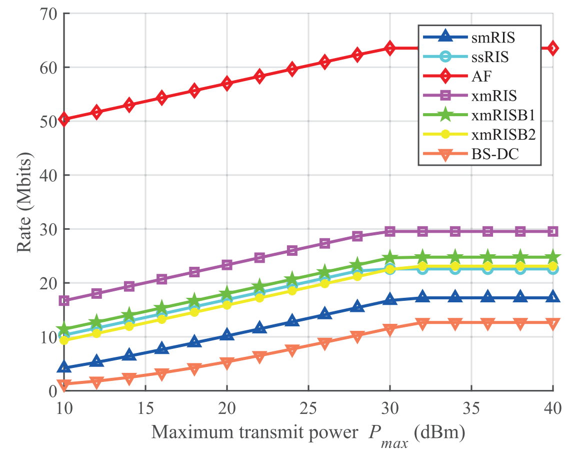

Fig. 7. Sum-rate versus the maximum transmit power.

Fig. 6 plots the change of energy efficiency versus maximum transmit power $P_{\max}$. The results show that the energy efficiency of the four schemes first increase and then tend to stable as the maximum transmit power increases. The energy efficiency stabilizes when $P_{\max} \geq 30$ dBm, which is because the objective function is convex and there exists a unique Optimal solution. In Fig. 6, we observe that the optimal transmit power is the maximum transmit power when $P_{\max} < 30$ dBm and remains constant when $P_{\max} \geq 30$ dBm. Therefore, in order to maximize the energy efficiency, the transmit power should be selected as 30 dBm. Fig. 6 also shows that the xmRIS scheme proposed in this article outperforms the smRIS, ssRIS, and AF schemes in terms of energy efficiency. Compared with smRIS, ssRIS, and AF schemes, the energy efficiency of xmRIS increases by 25%, 16%, and 40%, respectively. When disaster occurs in the communication link, the energy efficiency of the xmRIS blocking scheme is still higher than that of the smRIS, ssRIS, and AF schemes.

Fig. 7 shows the variation of the rates when changing the maximum transmit power $P_{\max}$. The results show that the rates of the four scenarios first increase Increase in logarithmic function trend and then tend to stabilize when the communication links are all working properly. This is due to the rate $R = B\log_2(1 + cp)$. We also consider the priority of energy efficiency, when $P_{\max} < 30$ dBm, the optimal transmit

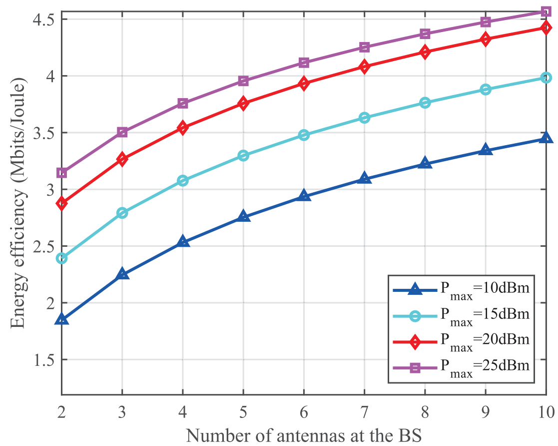

Fig. 8. Energy efficiency versus the number of transmit antennas at the BS.

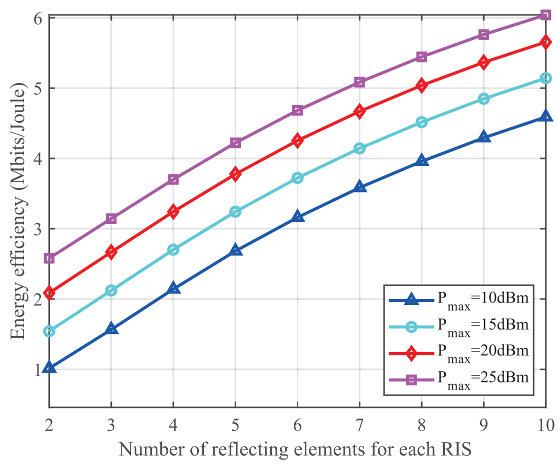

Fig. 9. Energy efficiency versus the number of reflecting elements for each RIS.

power increases with $P_{\max}$, and when $P_{\max} \geq 30$ dBm, the optimal transmit power and rate remain constant. It can also be observed from Fig. 7. The AF scheme has the highest rate because AF relays are active terminals, while RIS is a passive reflective structure. The xmRIS scheme proposed in this article outperforms the smRIS and ssRIS schemes in terms of rate performance due to the fact that the xmRIS scheme utilizes more communication links to complete the information transmission when transmitting the same information. Fig. 7 also shows that the xmRIS blocking scheme, although slightly lower than the xmRIS scheme in terms of rate performance, still outperforms the smRIS, ssRIS scheme.

Fig. 8 shows the relationship between energy efficiency and the number of BS antennas. From Fig. 8, we observe that with the increasing the number of BS antennas, the energy efficiency of xmRIS increases, and the growth trend becomes slower. This is because when the number of BS antennas increases, the BS power consumption increases faster and the growth rate of transmission rate gradually becomes slower, which slows down the growth trend of energy efficiency. It can also be seen from Fig. 8 that the energy efficiency keeps getting larger as the maximum transmit power $P_{\max}$ increases. The larger $P_{\max}$ is, the slower the energy efficiency growth is.

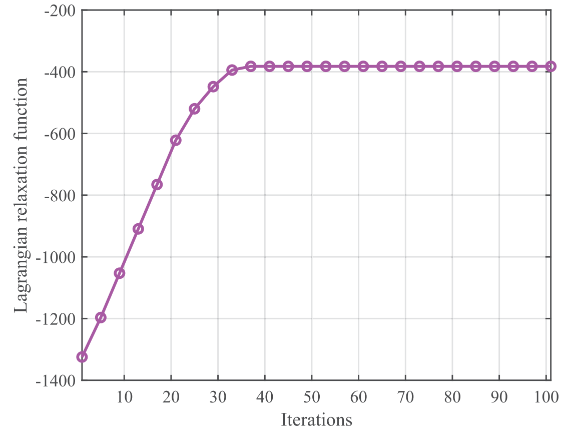

Fig. 10. Convergence of the objective function.

Fig. 9 shows the relationship between the energy efficiency and the number of RIS reflector elements. From Fig. 9, the energy efficiency of xmRIS increases linearly with the increase of RIS reflective elements. For the xmRIS proposed in this article, the appropriate number of reflective elements can be selected for each RIS according to the actual situation of the scenario.

Fig. 10 shows the method of solving the dual problem of sensing rate using the Lagrangian relaxation method. As observed from Fig. 10, the objective function (38a) gradually increases as the number of iterations increases and finally convergence. The convergence value at this point is the minimum value of the original problem (37a), and the opposite of this value is the maximum of the total sensing rate, the corresponding scheme at this point is also the optimal allocation scheme.

VII. Conclusion

In this article, energy efficiency of communication and sensing rate is optimized for multihop RISs-aided JCAS system in the coal mine scenario. In addition, we also investigate the robustness of the system. The energy efficiency of the communication system is improved by jointly optimizing the transmit power, the phase shift matrices and the RISs switches under the minimum rate and the maximum transmit power requirement. The total sensing rate is optimized under the constraints of sensing accuracy and transmit power. Simulation results show that the scheme outperforms the conventional AF scheme in terms of energy efficiency and disaster resistant. In summary, this article provides a possibility and feasibility of a vertical application for RIS and JCAS technologies.

References

[1] K.-G. Zhao and Y.-P. Li, "Analysis and development suggestion for coal resources safety in China," *Coal Eng.*, vol. 50, no. 10, pp. 185–189, 2018.

[2] Z. Xusheng, M. Guolong, Q. Wei, and N. Xiaoliang, "Early-warning index system of coal and gas outburst based on fault tree analysis," *Min. Safety Environ. Protect.*, vol. 46, no. 3, pp. 37–43, 2019.

[3] J. Song, Y. Zhu, and F. Dong, "Automatic monitoring system for coal mine safety based on wireless sensor network," in *Proc. Cross Strait Quad-Regional Radio Sci. Wireless Technol. Conf.*, vol. 2, 2011, pp. 933–936.

[4] M. Li and Y. Liu, "Underground coal mine monitoring with wireless sensor networks," *ACM Trans. Sensor Netw.*, vol. 5, no. 2, pp. 1–29, 2009.

[5] L. Muduli, P. K. Jana, and D. P. Mishra, "A novel wireless sensor network deployment scheme for environmental monitoring in longwall coal mines," *Process Saf. Environ. Protect.*, vol. 109, pp. 564–576, Jul. 2017.

[6] X. Xusheng, M. Kun, M. Hongwei, S. Wanfeng, and F. Hongwei, "Analysis of wireless electromagnetic wave propagation mechanism for coal mine rescue robot," in *Proc. IEEE Int. Conf. Real-Time Comput. Robot. (RCAR)*, 2018, pp. 64–67.

[7] I. B. Mabrouk, J. Hautcoeur, L. Talbi, M. Nedil, and K. Hettak, "Feasibility of a Millimeter-wave MIMO system for short-range wireless communications in an underground gold mine," *IEEE Trans. Antennas Propag.*, vol. 61, no. 8, pp. 4296–4305, Aug. 2013.

[8] C. Huang et al., "Multi-hop RIS-empowered terahertz communications: A DRL-based hybrid beamforming design," *IEEE J. Sel. Areas Commun.*, vol. 39, no. 6, pp. 1663–1677, Jun. 2021.

[9] G. Brooker, J. Martinez, and R. Hennessey, "Millimetre wave radar imaging of mining vehicles," in *Proc. 7th Eur. Radar Conf. (EuRAD)*, 2010, pp. 284–287.

[10] G. Brooker, E. Widzyk-Capehart, S. Scheding, R. Hennessy, and C. Lobsey, "Millimetre wave radar visualisation in mines," in *Proc. Eur. Radar Conf. (EuRAD)*, 2007, pp. 417–420.

[11] M. Leingartner, J. Maurer, G. Steinbauer, and A. Ferrein, "Evaluation of sensors and mapping approaches for disasters in tunnels," in *Proc. IEEE Int. Symp. Safety, Security, Rescue Robot. (SSRR)*, 2013, pp. 1–7.

[12] Q. Wu, Y. Zhao, Q. Fan, P. Fan, J. Wang, and C. Zhang, "Mobility-aware cooperative caching in vehicular edge computing based on asynchronous federated and deep reinforcement learning," *IEEE J. Sel. Topics Signal Process.*, vol. 17, no. 1, pp. 66–81, Jan. 2023.

[13] Z. Ding et al., "A state-of-the-art survey on reconfigurable intelligent surface-assisted non-orthogonal multiple access networks," *Proc. IEEE*, vol. 110, no. 9, pp. 1358–1379, Sep. 2022.

[14] L. Lv, Q. Wu, Z. Li, Z. Ding, N. Al-Dhahir, and J. Chen, "Covert communication in intelligent reflecting surface-assisted NOMA systems: Design, analysis, and optimization," *IEEE Trans. Wireless Commun.*, vol. 21, no. 3, pp. 1735–1750, Mar. 2022.

[15] Y. Liu, X. Mu, R. Schober, and H. V. Poor, "Simultaneously transmitting and reflecting (STAR)-RISs: A coupled phase-shift model," in *Proc. IEEE Int. Conf. Commun. (IEEE ICC)*, 2022, pp. 2840–2845.

[16] J. Yao, Z. Zhang, X. Shao, C. Huang, C. Zhong, and X. Chen, "Concentrative intelligent reflecting surface aided computational imaging via fast block sparse Bayesian learning," in *Proc. IEEE 93rd Veh. Technol. Conf. (VTC-Spring)*, 2021, pp. 1–6.

[17] K. Chen et al., "Recent advances in data-driven wireless communication using Gaussian processes: A comprehensive survey," *China Commun.*, vol. 19, no. 1, pp. 218–237, Jan. 2022.

[18] X. Tong et al., "Environment sensing considering the occlusion effect: A multi-view approach," *IEEE Trans. Signal Process.*, vol. 70, pp. 3598–3615, 2022.

[19] Y. Xu, H. Xie, Q. Wu, C. Huang, and C. Yuen, "Robust max-min energy efficiency for RIS-aided HetNets with distortion noises," *IEEE Trans. Commun.*, vol. 70, no. 2, pp. 1457–1471, Feb. 2022.

[20] T. Guo et al., "Joint communication and sensing design in coal mine safety monitoring: 3D phase beamforming for RIS-assisted wireless networks," *IEEE Internet Things J.*, early access, Feb. 9, 2023, doi: 10.1109/JIOT.2023.3242340.

[21] Y. Zhu and G. You, "Monitoring system for coal mine safety based on wireless sensor network," in *Proc. Cross Strait Quad-Regional Radio Sci. Wireless Technol. Conf. (CSQRWC)*, 2019, pp. 1–2.

[22] Y. Liu et al., "Reconfigurable intelligent surfaces: Principles and opportunities," *IEEE Commun. Surveys Tuts.*, vol. 23, no. 3, pp. 1546–1577, 3rd Quart., 2021.

[23] A. Zappone, P. Cao, and E. A. Jorswieck, "Energy efficiency optimization in relay-assisted MIMO systems with perfect and statistical CSI," *IEEE Trans. Signal Process.*, vol. 62, no. 2, pp. 443–457, Jan. 2014.

[24] K. V. Mishra, M. B. Shankar, V. Koivunen, B. Ottersten, and S. A. Vorobyov, "Toward Millimeter-wave joint radar communications: A signal processing perspective," *IEEE Signal Process. Mag.*, vol. 36, no. 5, pp. 100–114, Sep. 2019.

[25] F. Liu and C. Masouros, "Hybrid beamforming with sub-arrayed MIMO radar: Enabling joint sensing and communication at mmWave band," in *Proc. IEEE Int. Conf. Acoust., Speech Signal Process. (ICASSP)*, 2019, pp. 7770–7774.

[26] F. Liu, C. Masouros, A. P. Petropulu, H. Griffiths, and L. Hanzo, "Joint radar and communication design: Applications, state-of-the-art, and the road ahead," *IEEE Trans. Commun.*, vol. 68, no. 6, pp. 3834–3862, Jun. 2020.

[27] X. Tong, Z. Zhang, J. Wang, C. Huang, and M. Debbah, "Joint multi-user communication and sensing exploiting both signal and environment sparsity," *IEEE J. Sel. Topics Signal Process.*, vol. 15, no. 6, pp. 1409–1422, Nov. 2021.

[28] A. Zhang, M. L. Rahman, X. Huang, Y. J. Guo, S. Chen, and R. W. Heath, "Perceptive mobile networks: Cellular networks with radio vision via joint communication and radar sensing," *IEEE Veh. Technol. Mag.*, vol. 16, no. 2, pp. 20–30, Jun. 2021.

[29] F. Liu et al., "Integrated sensing and communications: Toward dual-functional wireless networks for 6G and beyond," *IEEE J. Sel. Areas Commun.*, vol. 40, no. 6, pp. 1728–1767, Jun. 2022.

[30] Y. Xu, H. Xie, D. Li, and R. Q. Hu, "Energy-efficient beamforming for heterogeneous industrial IoT networks with phase and distortion noises," *IEEE Trans. Ind. Informat.*, vol. 18, no. 11, pp. 7423–7434, Nov. 2022.

[31] Y. Liu, J. Xu, and X. Mu, "Fast beam splitting technique for STAR-RISs with coupled T&R phase shifts," in *Proc. 3rd URSI Atlantic Asia–Pacific Radio Sci. Meeting (AT-AP-RASC)*, 2022, pp. 1–3.

[32] Y. Ye, L. Shi, X. Chu, R. Q. Hu, and G. Lu, "Resource allocation in backscatter-assisted wireless powered MEC networks with limited MEC computation capacity," *IEEE Trans. Wireless Commun.*, vol. 21, no. 12, pp. 10678–10694, Dec. 2022.

[33] Y. Xu, G. Gui, H. Gacanin, and F. Adachi, "A survey on resource allocation for 5G heterogeneous networks: Current research, future trends, and challenges," *IEEE Commun. Surveys Tuts.*, vol. 23, no. 2, pp. 668–695, 2nd Quart., 2021.

[34] C. Shi, F. Wang, M. Sellathurai, J. Zhou, and S. Salous, "Power minimization-based robust OFDM radar waveform design for radar and communication systems in coexistence," *IEEE Trans. Signal Process.*, vol. 66, no. 5, pp. 1316–1330, Mar. 2018.

[35] A. R. Chiriyath, B. Paul, G. M. Jacyna, and D. W. Bliss, "Inner bounds on performance of radar and communications co-existence," *IEEE Trans. Signal Process.*, vol. 64, no. 2, pp. 464–474, Jan. 2016.

[36] C. Huang, A. Zappone, G. C. Alexandropoulos, M. Debbah, and C. Yuen, "Reconfigurable intelligent surfaces for energy efficiency in wireless communication," *IEEE Trans. Wireless Commun.*, vol. 18, no. 8, pp. 4157–4170, Aug. 2019.

Tianhao Guo (Member, IEEE) received the Ph.D. degree from the School of Electronic Engineering and Computer Science, Queen Mary University of London, London, U.K., in 2020.

He is currently a Lecturer with Shanxi University, Taiyuan, China. He is also the Postdoctoral Research Associate with the National Key Laboratory of Integrated Services Networks, Xidian University, Xi'an, China. His research interests include semantic and pragmatic communication, reconfigurable intelligent surface-aided joint communication and sensing in coal mines, and deep learning technologies for wireless communications.

Dr. Guo has reviewed papers from IEEE WIRELESS COMMUNICATIONS and WIRELESS COMMUNICATIONS AND MOBILE COMPUTING. He is also serving as a Review Editor in *Frontiers in Space Technologies* and *Frontiers of Computer Science*. He has served as the Workshop Co-Chair of ICSINC Big Data Workshop 2021.

Yujie Wang received the B.S. degree in science and technology of electronic information from Tangshan Normal University, Tangshan, China, in 2019. He is currently pursuing the M.S. degree in communication engineering with Shanxi University, Taiyuan, China.

Lexi Xu (Senior Member, IEEE) received the M.S. degree from Beijing University of Posts and Telecommunications, Beijing, China, in 2009, and the Ph.D. degree from the Queen Mary University of London, London, U.K., in 2013.

From 2013 to 2020, he was a Senior Engineer with the Network Technology Research Institute, China United Network Communications Corporation (China Unicom), Beijing. Since August 2020, he has been a Senior Engineer with Research Institute, China Unicom. He is also a China Unicom delegate in ITU, ETSI, 3GPP, Canadian Centre on Substance Abuse. He also serves as a Professor (part-time) with Beijing University of Posts and Telecommunications. His research interests include big data, self-organizing networks, satellite system, and radio resource management in wireless system.

Muyu Mei received the B.S. degree in applied mathematics from Xidian University, Xi'an, China, in 2017, where he is currently pursuing the Ph.D. degree in information and communication systems.

His research interests include performance analysis and stochastic optimization for large-scale wireless networks and multihop ad hoc networks.

Jia Shi (Member, IEEE) received the M.Sc. and Ph.D. degrees from the University of Southampton, Southampton, U.K., in 2010 and 2015, respectively.

From 2015 to 2017, he was a Research Associate with Lancaster University, Lancaster, U.K. From 2017 to 2018, he became a Research Fellow with 5GIC, University of Surrey, Guildford, U.K. Since 2018, he has been with Xidian University, Xi'an, China, where he is currently an Associate Professor with the National Key Laboratory of Integrated Services Networks. His current research interests include resource allocation in wireless systems, covert communications, physical layer security, mmWave communications, and satellite communications.

Dr. Shi is also serving as an Associate Editor for *Electronic Letters* and an Editor for *International Journal of Communication Systems*. He is serving as a Guest Editor for *China Communications*.

Lei Dong (Member, IEEE) received the Ph.D. degree in optics from Shanxi University, Taiyuan, China, in 2007.

From June 2008 to December 2011, he worked as a Postdoctoral Fellow with the Electrical and Computer Engineering Department and Rice Quantum Institute, Rice University, Houston, TX, USA. He is currently a Professor with the Institute of Laser Spectroscopy, Shanxi University. He has published more than 100 peer-reviewed papers with greater than 2200 positive citations. His research activities are focused on research and development in laser spectroscopy in the MIR and THz regions, in particular photoacoustic spectroscopy applied to sensitive, selective, and real-time trace gas detection, and laser applications in environmental monitoring, chemical analysis, industrial process control, and medical diagnostics.

Yongjun Xu (Senior Member, IEEE) received the Ph.D. degree (Hons.) in communication and information system from Jilin University, Changchun, China, in 2015.

He is currently an Associate Professor with the School of Communication and Information Engineering, Chongqing University of Posts and Telecommunications, Chongqing, China. From 2018 to 2019, he was a Visiting Scholar with Utah State University, Logan, UT, USA. He has authored or coauthored more than 100 papers, including IEEE Communications Surveys & Tutorials, IEEE Transactions on Communications, IEEE Transactions on Vehicular Technology, IEEE Wireless Communications Letters, and IEEE Communications Letters. His recent interests include resource allocation, intelligent reflecting surface, energy harvesting, backscatter communications, mobile edge computing, and UAV communications.

Dr. Xu received the Outstanding Doctoral Thesis of Jilin Province in 2016. He serves as an Associate Editor of *EURASIP Journal on Wireless Communications and Networking*, an Editor of *Physical Communication*, and an Academic Editor of *Digital Communications and Networks*. He serves as a Reviewer for IEEE Transactions on Wireless Communications, IEEE Transactions on Vehicular Technology, IEEE Journal on Selected Areas in Communications, and IEEE Transactions on Communications. He was the Technical Program Committee Member for many international conferences, such as GLOBECOM, ICC, ICCT, WCNC, ICCC, and CITS.

Chongwen Huang (Member, IEEE) received the B.Sc. degree from Nankai University, Tianjin, China, in 2010, the M.Sc. degree from the University of Electronic Science and Technology of China, Chengdu, China, in 2013, and the Ph.D. degree from Singapore University of Technology and Design (SUTD), Singapore, in 2019.

From October 2019 to September 2020, he is a Postdoctoral Fellow with SUTD. In September 2020, he joined the Zhejiang University, Hangzhou, China, as a tenure-track Young Professor. He is with the Zhejiang-Singapore Innovation and AI Joint Research Lab, Hangzhou, and the Zhejiang Provincial Key Laboratory of Info. Proc., Commun. and Netw. (IPCAN), Hangzhou. His main research interests are focused on holographic MIMO surface/reconfigurable intelligent surface, B5G/6G wireless communication, mmWave/THz communications, and deep learning technologies for wireless communications.

Dr. Huang is a recipient of the IEEE Marconi Prize Paper Award in Wireless Communications and the IEEE ComSoc Asia–Pacific Outstanding Young Researcher Award in 2021. He has been serving as an Editor of IEEE Communications Letters, *Signal Processing* (Elsevier), *EURASIP Journal on Wireless Communications and Networking*, and *Physical Communication* since 2021.